An Evaluation Study for Predicting Lithology and Pore Pressure from pre-stack seismic responses in the Porcupine Basin

Author:

Paul Haskey

Scott Pickford Group

prepared for

The Porcupine Study Group (PSG):

Agip,
Chevron,
Enterprise Oil,
Marathon,
Phillips,
Petroleum Affairs Division,
Statoil,
TotalFinaElf

June 2001

Contents

1. Summary

Starting from CMP gather data from seismic 2D line ST9506-421 and well data from well 35/18-1, the objectives of the seismic processing were to discriminate between the main lithologies in the target Lower Palaeocene section, and to investigate the possibility of predicting pressure variations along a sand formation (at depth 11700ft in the well). A third objective was later established to predict pore-pressure for the shale section identified along the profile. The potential for lithology discrimination and for predicting pore-pressure is based on methods of pre-stack inversion that allow the estimation of elastic properties such as the Lamé parameters. These can be transformed and cross-plotted to optimise the required discrimination between lithologies, fluids or pressure conditions as indicated by petrophysical analysis. Petrophysical analysis is also needed to show when the desired discrimination may be possible.

The method of pre-stack inversion depends on the availability of a reliable "macro" velocity model (representing the slow, background velocity variations), and much effort was expended in deriving different versions of this model. The final model was built using pre-stack depth migration based tomography. This gave the required temporal and spatial detail together with good agreement with the well velocities in the Palaeocene section. The macro-model for the s-wave was derived from the p-wave model using the Mason empirical relation in the absence of recorded s-wave log data.

Pre-stack inversion was performed in two steps, the first being an AVO analysis to derive estimates of p-wave and s-wave reflectivities. In the second phase, a model driven joint inversion algorithm was used to find globally optimised models for p-wave and s-wave impedance. Scaling, wavelets and parameterisation of the inversion were all checked at the well location for a satisfactory fit against well derived models before applying the inversion to the complete profile, but there is no way of forcing the fit in this method.

Petrophysical analysis showed that the Palaeocene sand unit could best be separated from other lithologies in a cross-plot of λ/μ against $\lambda*\rho$, where λ and μ are the Lamé parameters related to the incompressibility and rigidity of the rock respectively, and ρ is the density. This cross-plot was used to define the locations of the sand unit (or units) across the profile. The top of the sand and its thickness (in TWT) are predicted in very good agreement with the actual observed lithology at the well location. Other formations that are also probably sands are predicted at a shallower level, such as the unit seen at about 2.75s TWT occupying a region centred around SP420.

The analysis of pore-pressure effects on the palaeocene sandstone, using petrophysical modelling, showed that the changes in velocity (and hence elastic properties) induced by changes over the feasible range of pressures would be too small to be reasonably detectable at this depth. (Observed variations in the estimated elastic properties of the sand are more likely to be due to changes in pore-fluid properties). Instead we used the lithology discrimination to extract a shale section and then predicted pore-pressure for the shales using the Eaton relationship applied to the

detailed velocity model derived from the seismic inversion. This approach predicted pore-pressures that were in good agreement with an Eaton calculation applied to the well data. In particular the method predicts the presence of an over-pressured shale just above the Top Chalk at a depth of approximately 12000 ft. This shale appears to be continuous across much of the 2D profile represented by this seismic line. There also appears to be a thicker band of lower velocity shales in a zone above the sand centred at a TWT of around 2.8s. This band again extends more or less uniformly across the section. (Figure 15).

2. Objectives

The aims of the seismic reprocessing were:

1. Determine whether it is possible to discriminate between lithologies from the pre-stack seismic responses and apply this discrimination to distinguish sands from shales (and carbonates) across the section.
2. Apply the results of petrophysical analysis to the estimation of pore-pressure in the palaeocene sand.
3. At a later stage a further objective was added – to estimate and display pore-pressure in the shale section of the lower palaeocene. A low velocity shale unit was observed in the well at a depth of 12000ft just above Top Chalk. The question asked was whether it was possible to recognise this unit as an over-pressured shale in the seismic response and image it within the 2D section.

Input Data

The data available for this study were essentially seismic data for the 2D line ST9506-421 and well data for the well 35/18-1.

The seismic data were in the form of partially processed CMP gathers, covering a SP range 101-450 (CMPs 320 - 1720 using the numbering from the original processing – by Robertson Research). The gathers as delivered were 80 fold with a maximum offset of just over 4 km.

The well is located on the seismic line near CDP610. Well data consisted of a full suite of logs (although no shear wave sonic data was available), and included RFT data for the target sand, but no pressure values were available for the shale formations.

3. Seismic Pre-processing

The input CMP gathers had already had some limited pre-processing, which included a Radon demultiple and DMO. The important issues for the purposes of this project were to ensure that the image was well focused in the pre-stack domain prior to AVO and inversion, that the amplitudes were well conditioned for pre-stack inversion, that the traces were zero-phased relative to reflectivity at the well, and that the signal spectrum was as broad as the signal/noise ratio would allow.

These considerations resulted in the following processing sequence:

1. Pre-stack Time Migration. NMO was removed to allow velocity analysis (below).
2. Random noise attenuation by FX Deconvolution applied to common offset gathers.
3. Stack the gathers and perform wavelet estimation by partial coherence matching against the well synthetic seismogram. (Corrective phase-shift applied prior to AVO and Inversion. The wavelet estimated was already close to zero-phase, and the phase correction applied subsequently was only 8deg). In making this tie, a time shift of close to 40deg was observed between the calibrated well trace and the matching seismic signal. The tie seems to be unambiguous in the window of data available for this analysis (at all levels, although the tie at the earlier times is fairly poor). This may lead one to suspect some possible problem with the check-shot data. (Figure 1).
4. Intensive velocity analysis was performed, tied to main horizons. Accurate NMO is needed for the AVO analysis, and these intensive velocities were also used for building one of the velocity models to be used for inversion (below). (Figure 2).
5. Amplitude corrections (already applied) were checked by comparing the p-wave and s-wave reflectivity estimated from the AVO equation against the corresponding synthetics at the well. A gain curve was applied to the reflectivity estimates. Slightly different scalars were needed for the two reflectivities going into the joint inversion process, correcting, together with the residual gain curve, for some inaccuracy in the original amplitude conditioning.

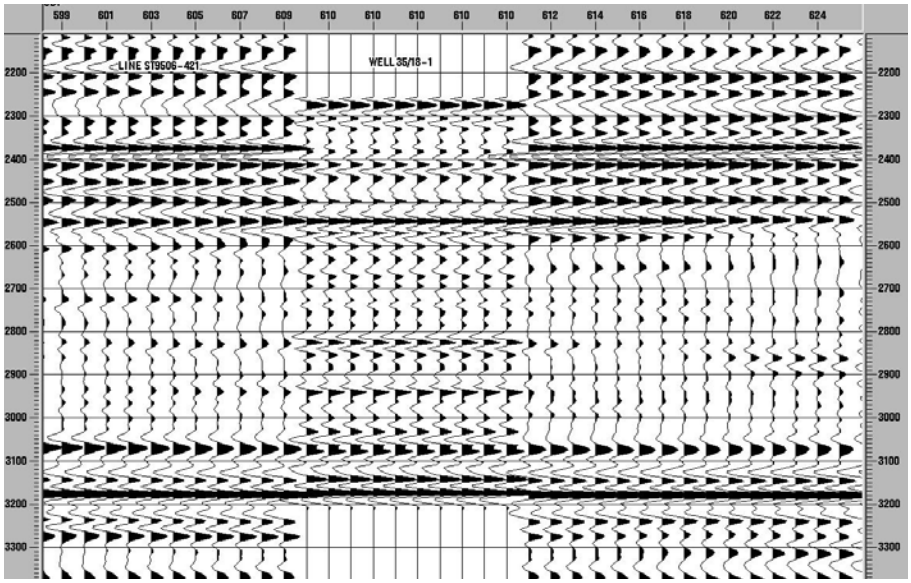

Figure 1. Seismic and well synthetic traces with estimated wavelet applied to log reflectivity

4. Velocity Model Building

An initial, simple velocity model was built by mapping the smoothed velocity log across the section following key marker horizons. With many wells this simple method can provide a satisfactory reference model for AVO and Inversion. In this case there is only one well, which gave rise to some concern for recognising spatial variations and including them in the model.

The low velocity zone between the sand and the Top Chalk showed as a low velocity interval in the seismic velocity analysis at the well. The results of intensive seismic velocity analysis – for optimum NMO – were therefore used to build a second velocity model which should include any meaningful spatial variations. In this seismic velocity model there are not many indications of the low velocity zone at the base of the palaeocene except in the zone around the well. (Figure 3).

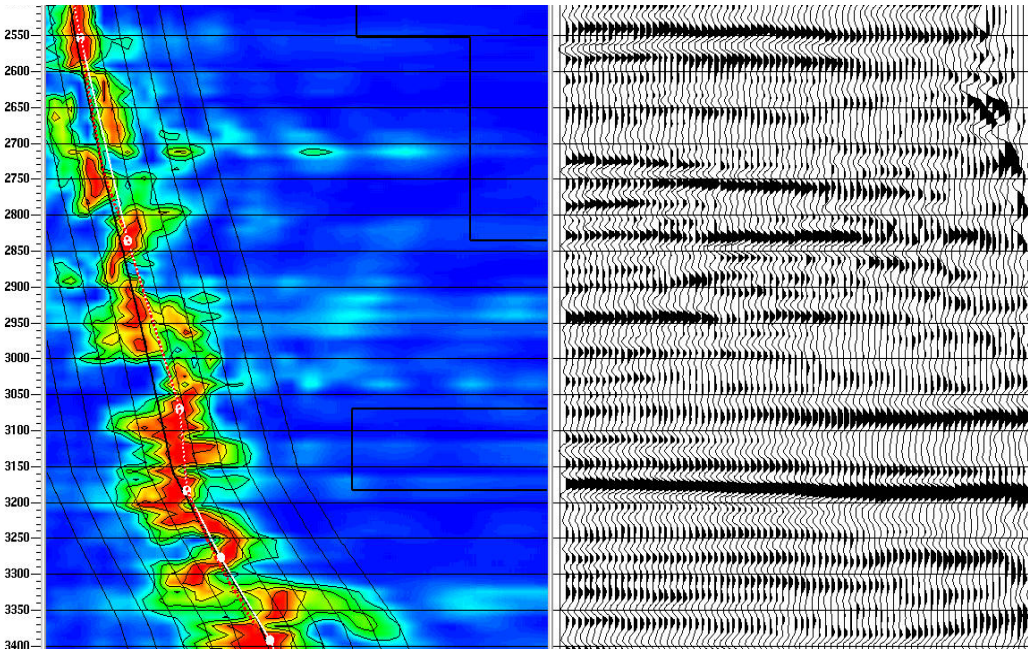

Figure 2. Seismic velocity at the well location. Top sand is at 3050ms.

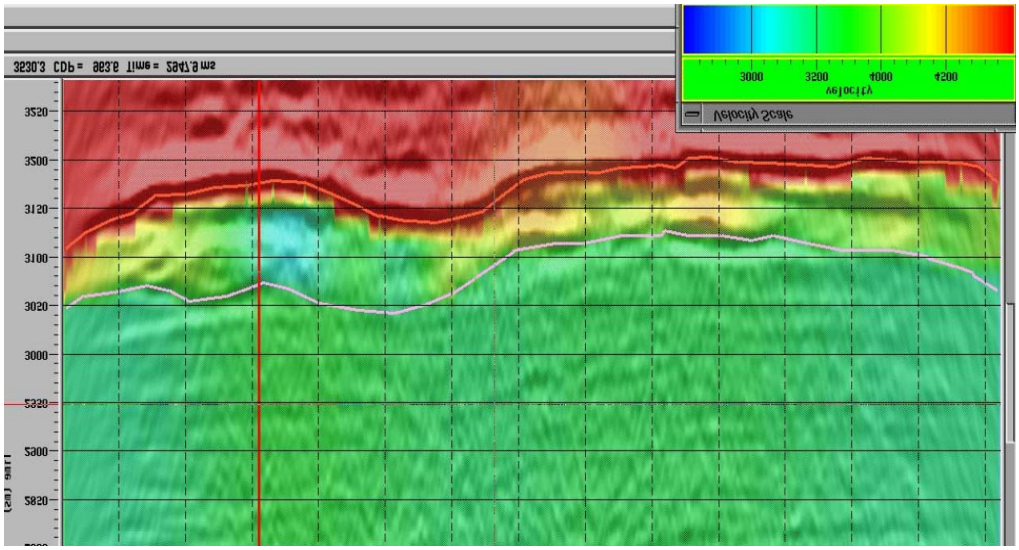

Figure 3. Velocity model from conventional seismic velocity analysis (Lower Palaeocene and Upper Chalk)

Both p-wave and s-wave macro-models are needed. The empirical Mason relation used at the well to estimate s-wave from p-wave velocity was applied to the full macro models.

In the inversion these models act as "soft" constraints only, the seismic amplitudes providing much more information, and particularly the details of the final estimated impedance models. However it is clear that estimates of pore-pressure derived from inversion results, particularly for the shales, do depend considerably on the accuracy of the background model used to constrain the process.

A density profile was needed for creating macro models of seismic impedance. This was again generated from the well data by mapping a smoothed version across the picked horizons.

5. AVO and Inversion

The zero-phase time migrated gathers with intensive NMO corrections were input to a two stage inversion process. It is possible to perform this inversion in a single pass, but there are some advantages in being able to review the results of estimating the p-wave and s-wave reflectivity profiles, derived from the Fatti AVO equation, prior to the second inversion step.

Angles of propagation are determined by ray tracing through the smooth p-wave macro-model. AVO analysis with this equation (accurate to about 45deg) was performed with maximum angles of incidence of about 40deg. Noise levels were deteriorating at angles wider than this. (Figure 4).

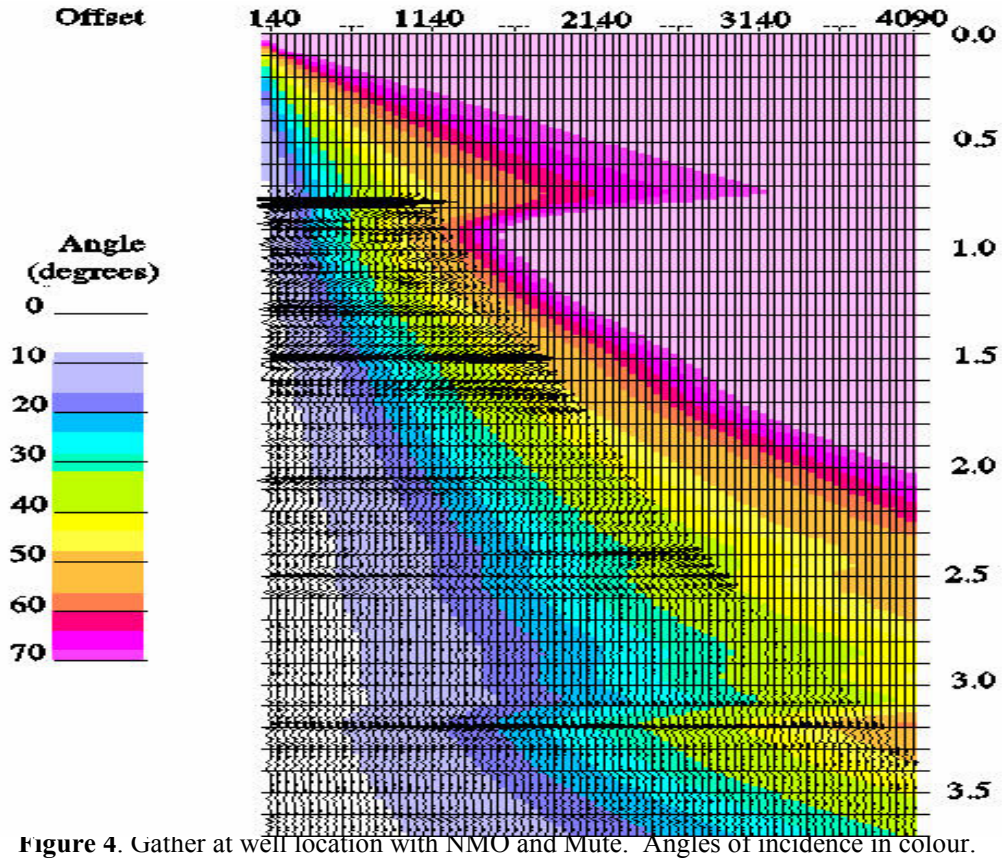

Figure 4. Gather at well location with NMO and Mute. Angles of incidence in colour.

The Fatti equation estimates p-wave and s-wave reflectivities directly as coefficients of the angle dependant terms. The reflectivity images were treated with random noise attenuation in the form of FX "Deconvolution". Spectral shaping was applied in a frequency domain deconvolution to broaden the spectrum and to improve its consistency across the section. The reflectivity estimates were then compared against well-derived synthetic seismograms to verify the phase and amplitudes of each component, prior to performing the elastic inversion. No further adjustments were made to the phase of the reflectivity signals.

A final verification of the wavelet and amplitudes was achieved by trial inversions of traces around the well, testing small variations in scaling and phase around the values determined for matching the reflectivity data. (Figure 5).

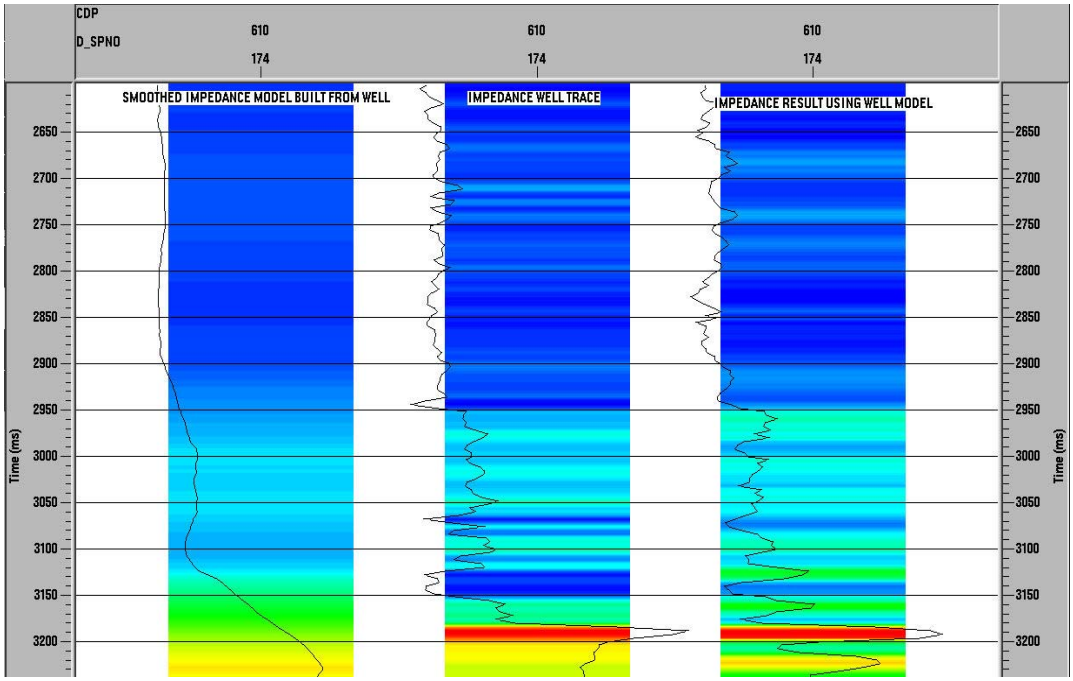

Figure 5. Trial of joint inversion at well location

The inversion of reflectivity data to p-wave and s-wave impedance estimates was performed with a joint inversion algorithm, building a common model for the two impedance components – p-wave and shear wave. Besides the reflectivity data, the inputs to this process are the estimated wavelets and the macro-models derived as described previously. The task of the inversion algorithm is to find the impedance model(s) that deliver convolution seismic responses which match the observed seismic reflectivity responses, applying constraints derived from the macro-models. The differences between the estimated and the *a priori* models are also used as a weighted component of the cost function minimised by the process. The Vs/Vp ratio of the derived model(s) provides a further, similar soft constraint. A global minimum for the cost function is found by the directed search process of simulated annealing.

The outcome of this process is a pair of models for p-wave and s-wave impedance. The constrained global optimisation approach produces results which are both high resolution and stable. (Figures 6 and 7).

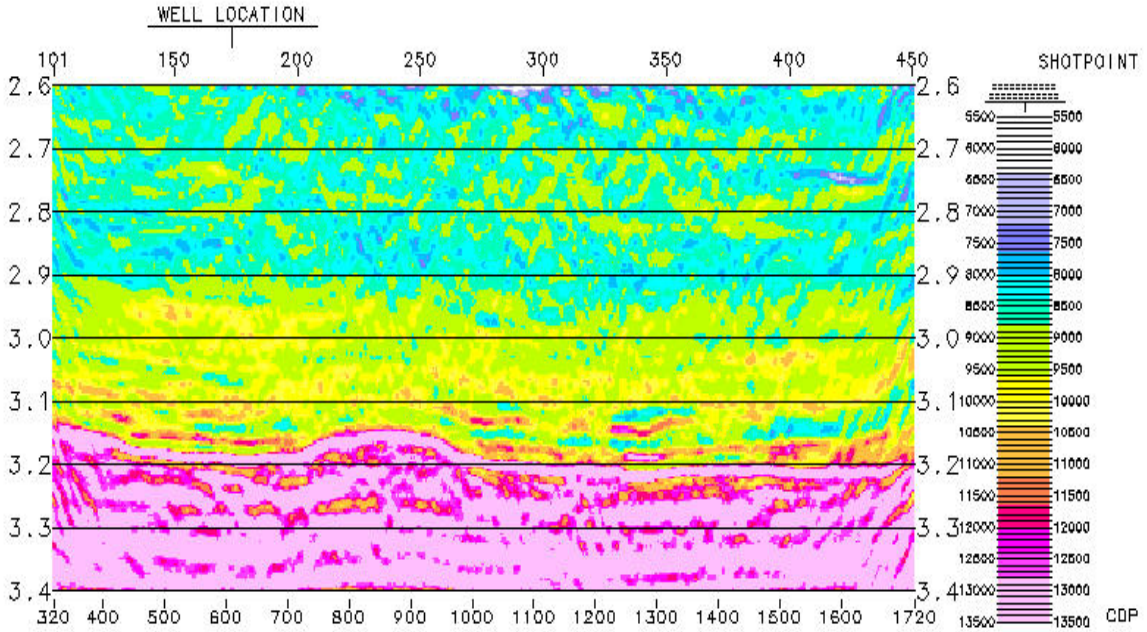

Figure 6. P-impedance from joint inversion. A priori model from well data

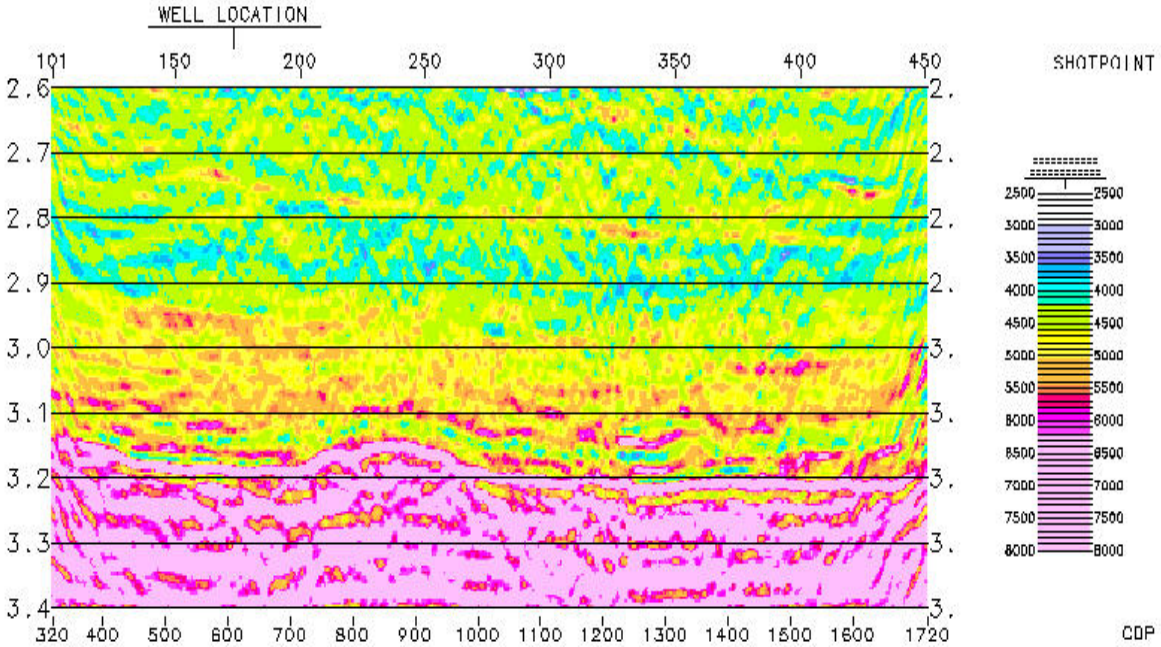

Figure 7. Shear impedance from joint inversion with result in Fig 6.

The macro-models derived in the different ways described above delivered inversion results that were quite similar for the most part, but the differences that did show up

were possibly very significant, since the model derived from the seismic analysis was seeing variations in velocity along the profile in the interval just above top Chalk, including the Palaeocene sand.
The parameters finally used for lithology discrimination proved fairly insensitive to these variations – a good indicator for the reliability of this discrimination (section 7), but the requirement for pore-pressure prediction was the detailed velocity model itself which clearly is sensitive to the *a priori* model used in the inversion. We decided that a further look at the velocity field was needed, with a more focused approach than the analysis based on preliminary pre-stack time migration.

6. Further Velocity Modelling - Pre-stack Depth Migration and Tomography

In this approach, pre-stack depth migrated gathers are picked for residual errors along key picked horizons. The errors are then resolved in a reflection tomography solution. The model for initial depth migration was the well-derived model, so the tomography solution is looking for departures from this model. In general it was found that the velocities in the shallower section, with only check-shot control, needed to be speeded up to optimise the depth imaging. Having done this, the variation across the profile at the Lower Palaeocene level was not so strong as suggested by the original PSTM velocity analysis. The low velocity zone between the sand and the Top Chalk now looks more consistent. This leads to an inversion result in which there is good resolution of the low velocity shale near the base of the palaeocene section. (section 8)

7. Lithology Prediction

The options for discriminating between sandstone, shales and carbonates were examined in cross-plots from both the log data and the elastic parameters derived from the seismic images. The transformations to Lamé parameters λ and μ (strictly λ*ρ and μ*ρ) are relatively straightforward, where λ and μ are related to the incompressibility and rigidity of the rock respectively, and ρ is the density. (Figure 8).

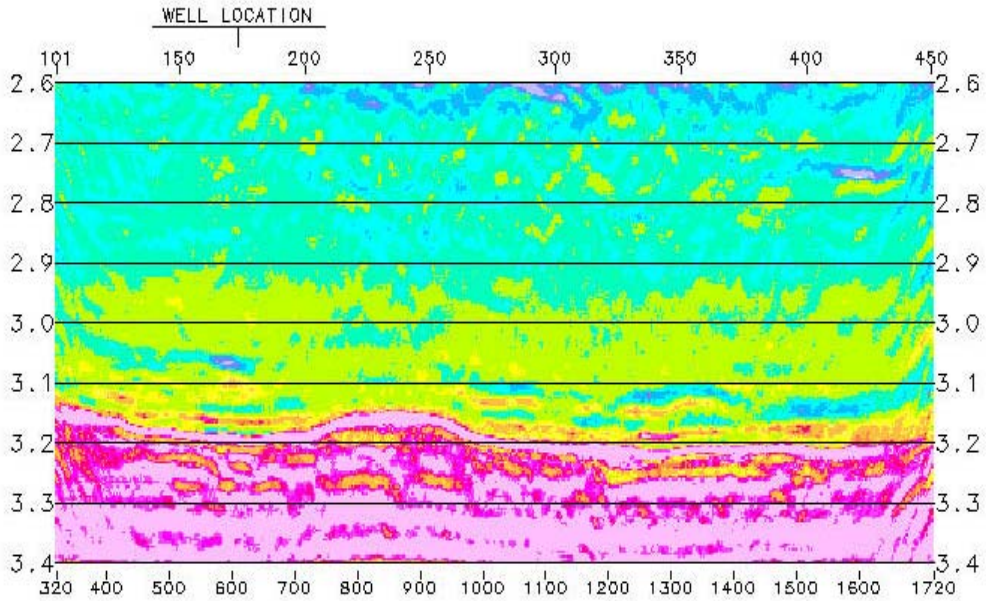

Figure 8. Section of λ*ρ parameter from joint elastic inversion. The Palaeocene sand is seen as a feature with low λ*ρ values at 3050ms at the well location. Similar units appear to the right of the Chalk high. Low values are shown in cold colours.

The Lamé parameters can be combined to compute highly fluid and/or lithology sensitive parameters such as the ratio of λ / μ. The petrophysical examination showed that the cross-plot of this ratio against λ*ρ was a very effective way of separating the sand from the other lithologies (Figure 9). This is generally a good sand indicator, since the clean sands usually have lower values of λ (more compressible) and higher values of μ (rigidity) than the shales at similar depths. The cross-plot can be used to pick out and display the sand selectively. Making λ*ρ the parameter actually displayed can then highlight the zones where the pore fluids may be more prospective. Gas sands will show as particularly strong anomalies with this parameter, which is very sensitive to fluid incompressibility.

Selecting the lower left portion of the cross-plot of the transformed seismic traces it was quite straightforward to verify that the sand was predicted from the seismic parameters at the time and thickness expected at the well location (Figure 10 and 11). Identification of carbonates is much more straightforward. In the pore-pressure analysis described in section 8 both sands and carbonates were masked off to produce an estimated shale-only section.

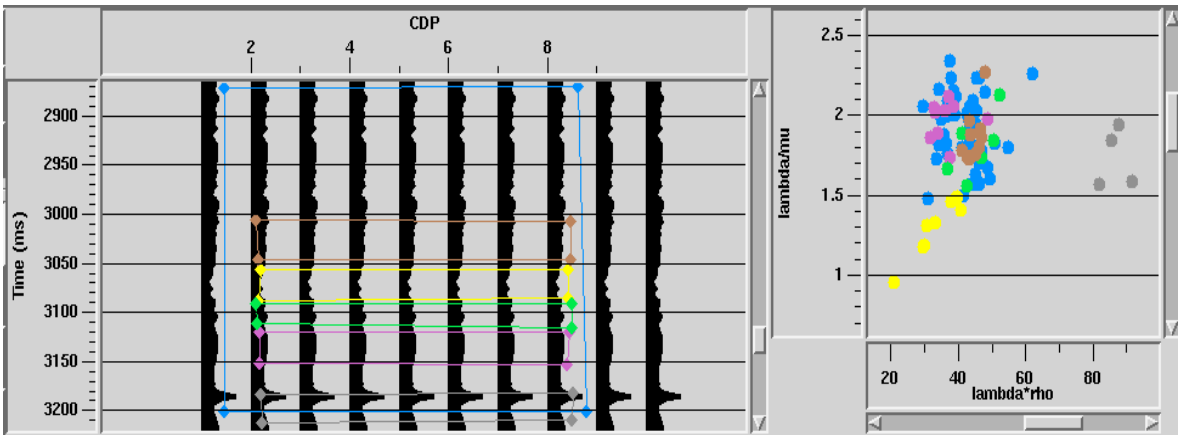

Figure 9. Cross plot of lambda/mu vs lambda*rho from the log data (repeated traces of lambda/mu shown). The sand unit is in the yellow zone. The deeper low velocity shale is the purple window.

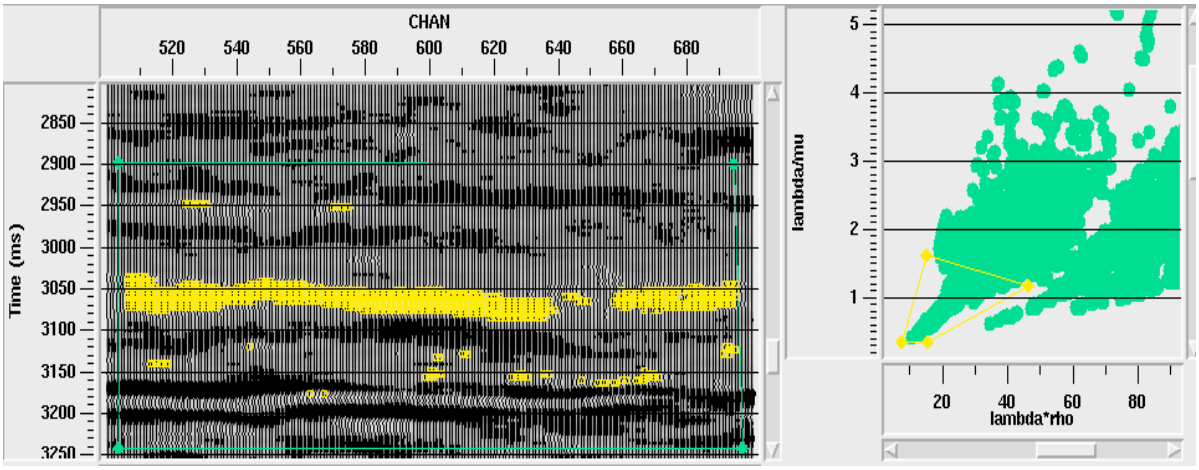

Figure 10. Cross plot of lambda/mu vs lambda*rho for the seismic profile around the well location. The selected zone in yellow corresponds well to the sand location and thickness.

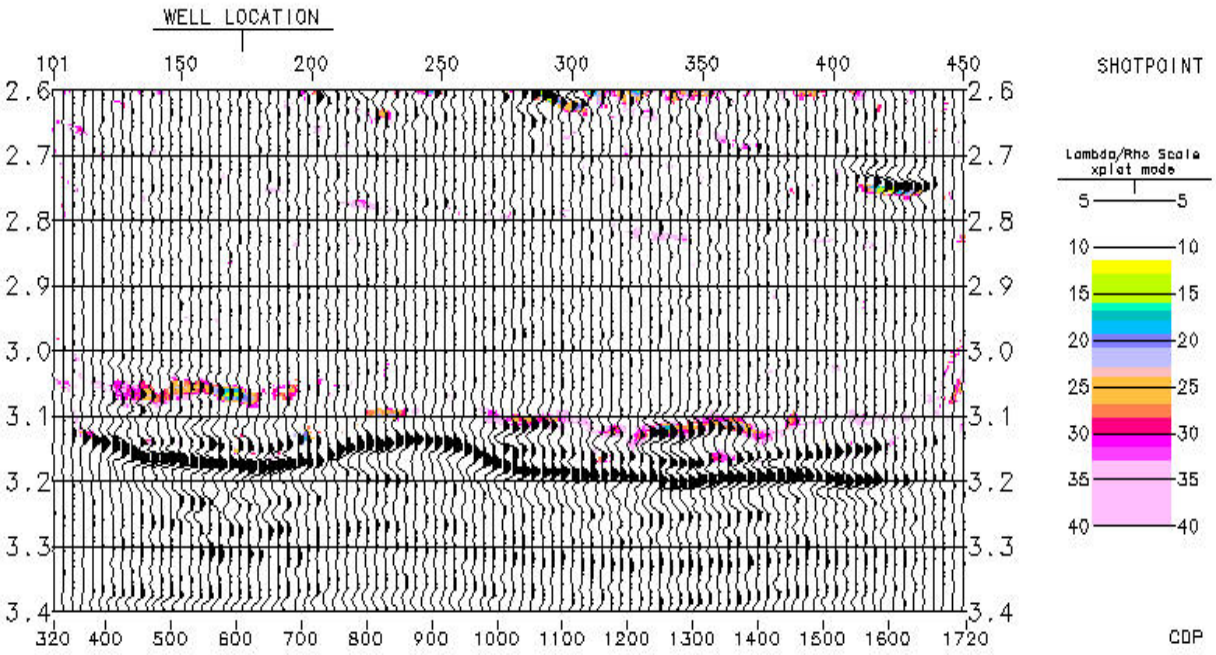

Figure 11. Sand zone section: cross-plotted selected region overplotted on the reflectivity image. The colour is the lambda*rho value.

8. Pore-pressure Prediction

Turning finally to the issue of pore-pressure estimation, the petrophysical analysis based on the log parameters and the RFT data for the sand showed that the sensitivity of velocity (and therefore elastic parameters) to pore-pressure changes over the range possible in the sand under investigation is very low, and almost certainly undetectable in the seismic responses. This was a disappointing conclusion. For enclosed sands this appears to be a case dependent situation. (A separate report by Thomas Schulte – attached - describes this investigation).

The shale section seemed to be more amenable to pore-pressure analysis, with the aid of the detailed velocity picture that is available from the combination of tomography analysis and seismic inversion. Cross-plotting Ip vs Is from the well data showed that the over-pressured shales tend to reside at the low end of both parameters – both acoustic and shear wave impedances are low (Figure 12). It was interesting to see whether sufficient resolution could be achieved in the velocity model to enable the thin low velocity shale below the sand to be seen and its pore-pressure estimated.

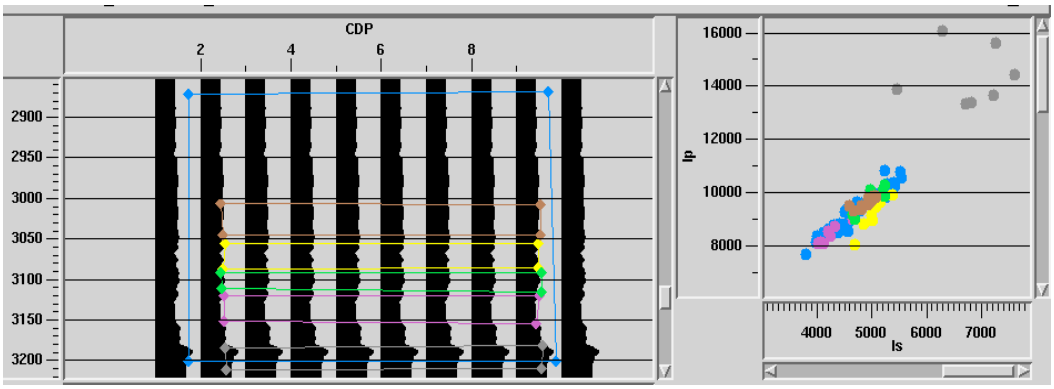

Figure 12. Plot of P-impedance vs Shear-impedance from log data. (Repeated)Trace shown is P-impedance. Coloured zones the same as Fig. 9.

For this purpose the main requirement is a detailed and reliable velocity model. Velocities were estimated from the derived p-impedance model by dividing by density values predicted from a Gardner type of exponential relationship between velocity and density. This was determined by cross-plotting the log data, using the shale lithologies only. The "inverse Gardner" relation was derived from this and applied to the p-impedance model to provide a detailed velocity model (Figure 13).
Error involved in the conversion of p-wave impedance to velocity is difficult to estimate, but it does seem that the lower velocity, over-pressured shales tend to drift towards lower values of density than the normal Gardner trend, which has a power exponent of around 0.25. i.e. $\rho \alpha V^{0.25}$. In this case the exponent is closer to 0.4 or slightly higher. This was used for the conversion.

The velocity model derived shows the expected detail in the lower palaeocene section, both the sand (about 3050ms at the well location) and the deeper low velocity shale (about 3130ms at the well location) being clearly visible. The shale extends most of the way across the section.

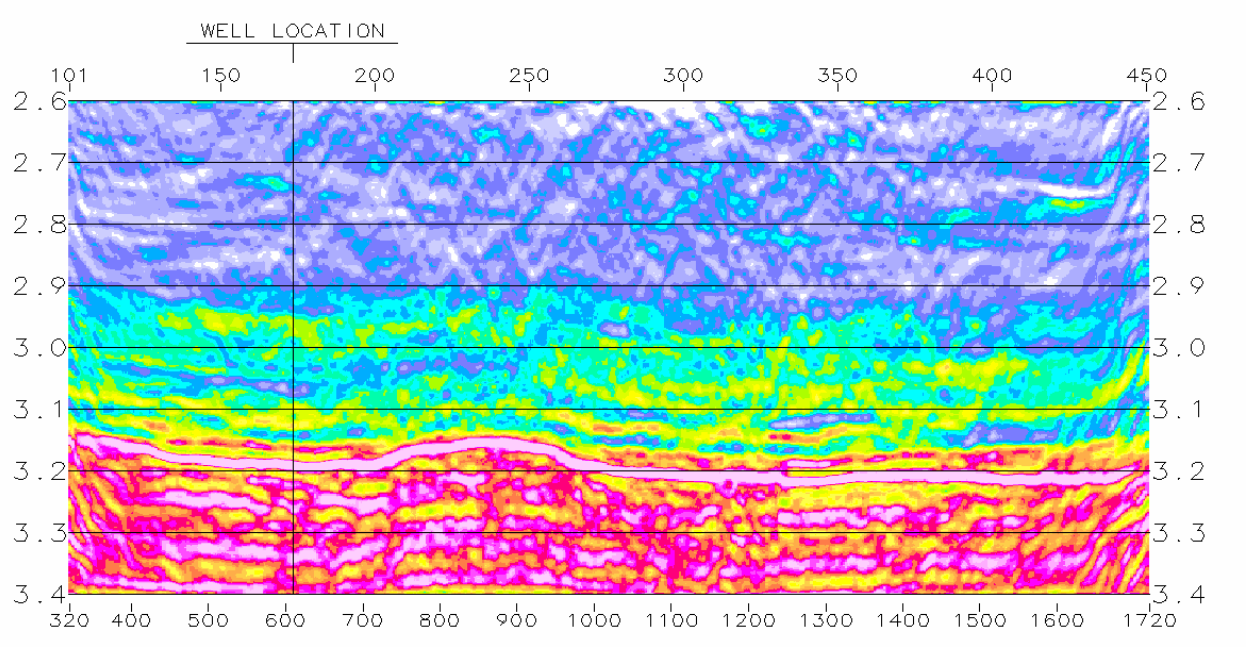

Figure 13. P-wave velocity model from tomography and inversion. Red high. Blue low

To convert this velocity field to estimated pore-pressure we applied the standard Eaton relation. For this purpose the geostatic gradient computed at the well was extrapolated as the reference column across the section, following the main interpreted horizons. This and the normal compaction trend in depth were converted to time for the pore-pressure calculations. The exponent used in the empirical relation was 3.0. Computations were performed for the shale section only, by removing the predicted sand and carbonate lithologies. The result is shown as a pore-pressure gradient in the form of both time and depth profiles. (Figures 14 and 15). There is good agreement at the well location with the equivalent calculation performed on the logs.

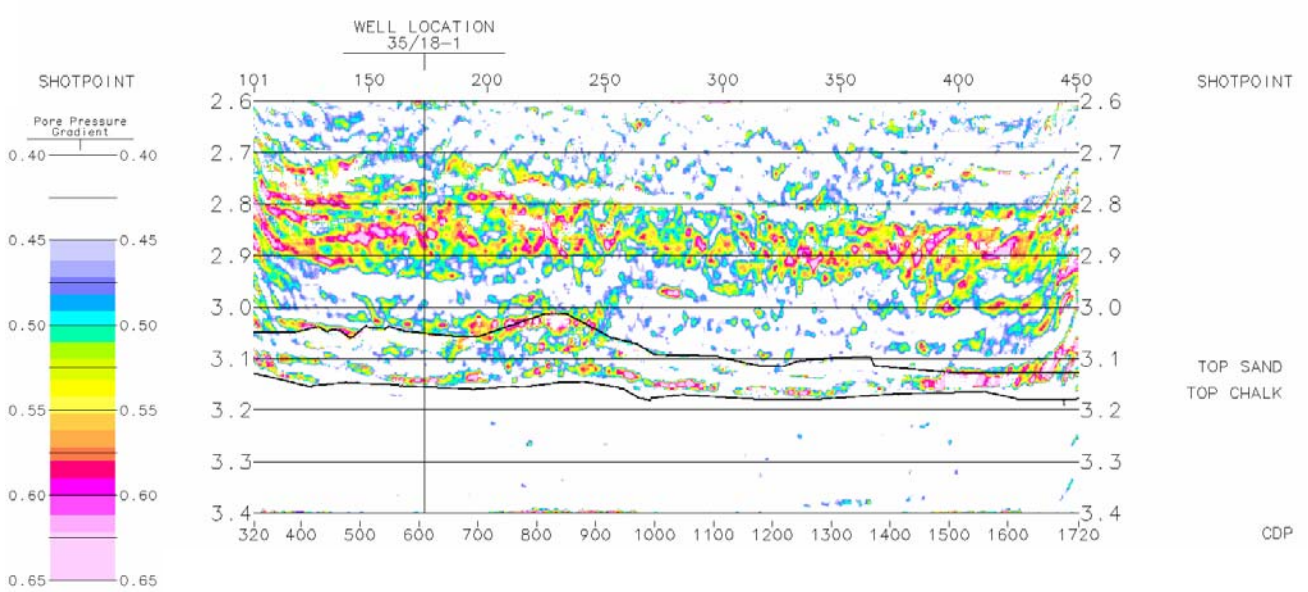

Figure 14. Predicted pore-pressure for the shale section. Other lithologies removed from the display. Displayed as a section in TWT.

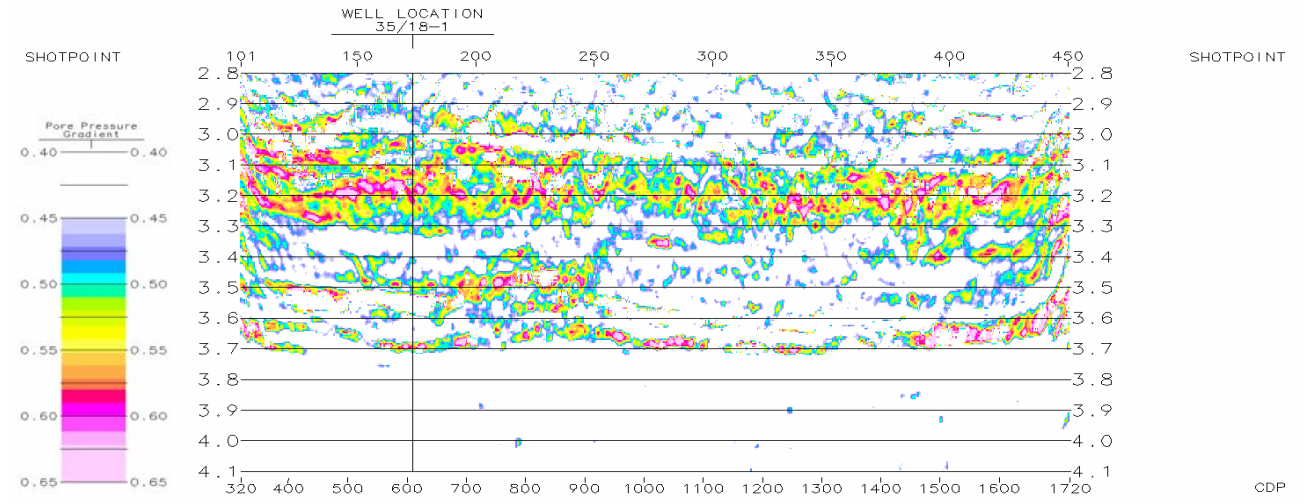

Figure 15. Predicted shale pore-pressure as a depth section. Depth in km.

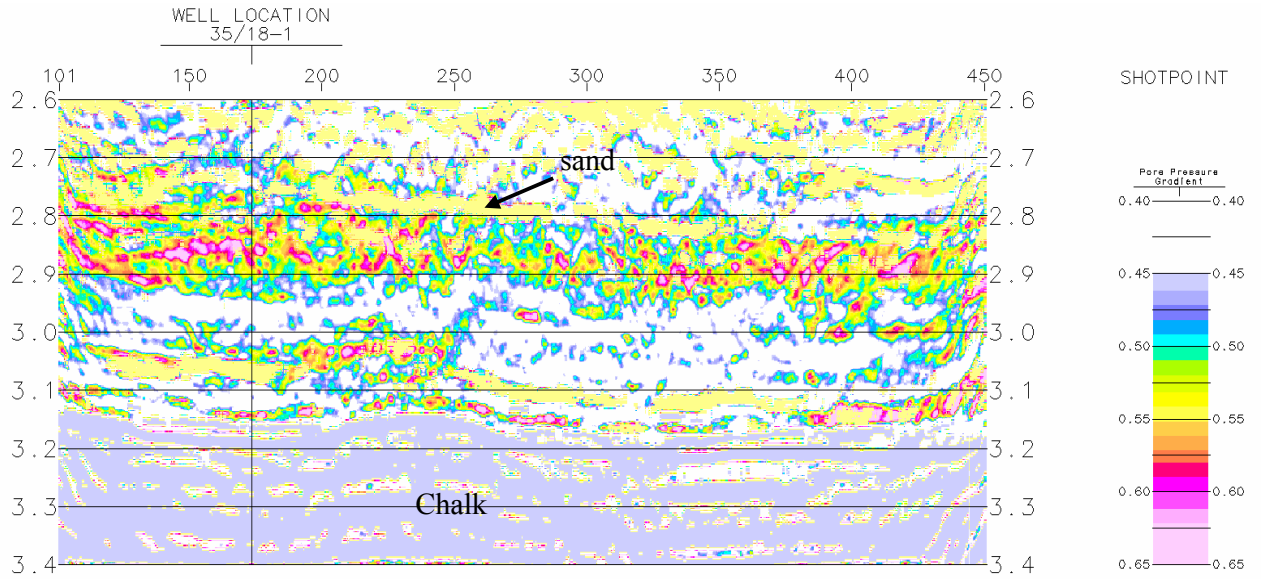

Figure 16. Predicted shale pore-pressure with sand and carbonate formations shown in yellow and grey colours respectively. Section in TWT.

9. Conclusions

The conclusions which can be drawn from this investigation into the recognition of pressure effects and discrimination of lithologies from seismic responses are as follows:

1. The pore-pressure of the palaeocene sand primarily investigated does not have enough effect on the seismic velocities for the possible variations to be detectable.
2. Pre-stack inversion and estimation of Lamé parameters enables cross-plotting to be used to discriminate between the sand and the shales at this depth. This works because the sands in this interval tend to show low values of the incompressibility parameter λ, and higher values of the rigidity modulus μ than shales at this depth. The lambda parameter is also very sensitive to pore fluid variations.
3. The discrimination of sands from shales enables pore-pressure to be calculated for the shale section using an Eaton or similar relationship based on the ratio of velocity for the normal compaction trend to the velocity observed. Shale pore-pressure and predicted lithologies can be displayed together (Figure 16).
4. Not surprisingly the macro or *a priori* velocity model is perhaps the most critical component of this inversion based procedure for pressure prediction. The method used finally in this case uses PSDM and reflection tomography. The result seems to offer a good compromise between reliability and resolution. The detail of the model is derived from the pre-stack reflection amplitudes. It is worth noting that when AVO effects are quite strong, such as observed at the top of the sand, a stack method to estimate acoustic impedance could give very misleading results, and there would be little or no prospect of the lithology discrimination which is essential for this approach.
5. As far as the original sand target is concerned there may be some mileage in the simple model that a porous sand in close contact with an overpressured shale is most likely to be over-pressured itself.

10. References

Fatti J.L., Smith G.C., Vail P.J., Strauss P.J. and Levitt P.R. 1994. *Detection of gas in sandstone reservoirs using AVO analysis: A 3D seismic case history using the Geostack technique.* Geophysics 59, 1362-1376.

Goodway W., Chen T. and Downton J. 1997. *Improved AVO fluid detection and lithology discrimination using Lamé parameters; "Lambda*Rho", "Mu*Rho" and "Lambda/Mu fluid stack", from P and S inversions.* 1997 CSEG meeting abstract, 148-151.

Ma X-Q. 2001. *A constrained global inversion method using an overparameterised scheme: Application to poststack seismic data.* Geophysics 66, 613-626

Ma X-Q. 2000. *Global Joint Inversion of Acoustic and Shear Impedance from Prestack Seismic Data.* SPG Technical Note 017.

11. APPENDIX

List of digital outputs: CGM+ files (*.CGM) and SEGY (.sgy) data

CGM files	File Name
Reflectivity Sections	
PSTM Stack	Pstm_stack.CGM
PSDM Stack converted to time	Psdm_stack.CGM
Impedance Sections	
P-Impedance - log derived macro model	Pimp_logvel.CGM
P-Impedance - macro model from seismic NMO velocities	Pimp_seisvel.CGM
P-Impedance - macro model from tomography	Pimp_psdmvel.CGM
S-Impedance - log derived macro model	Simp_logvel.CGM
S-Impedance - macro model from seismic NMO velocities	Simp_seisvel.CGM
S-Impedance - macro model from tomography	Simp_psdmvel.CGM
Lambda*Rho Sections	
Log derived macro model	LR_logvel.CGM
Macro model from seismic NMO velocities	LR_seisvels.CGM
Sand units predicted by cross-plot – lambda*rho plotted (log velocity model)	LR_xplot_log.CGM
Sand units predicted by cross-plot – lambda*rho plotted (tomography model)	LR_xplot__seisvels.CGM
Shale/Pore-pressure Profiles	
Velocity model from tomography + pre-stack inversion	PVEL_INT.CGM
Predicted shale section with estimated pore pressure (TWT)	EATON_PP_TIME.CGM
Predicted shale section with estimated pore pressure (Depth)	EATON_PP_DEPTH.CGM
Shale section with predicted sand and chalk added	PP_SAND_CHALK.CGM

SEGY files	File Name
Reflectivity Sections	
PSTM Stack	st9506_421_pstmstk_pickedvels.sgy
PSDM Stack converted to time	st9506_421_pstmstk_tomovels.sgy
Impedance Sections	
P-Impedance - log derived macro model	Pimp_No_smthdmod_well.sgy
P-Impedance - macro model from seismic NMO velocities	Pimp_No_smthdmod_Seisvels.sgy
P-Impedance - macro model from tomography	Pimp_psdmvels.sgy
S-Impedance - log derived macro model	Simp_No_smthdmod_well.sgy
S-Impedance - macro model from seismic NMO velocities	Simp_No_smthdmod_Seisvels.sgy
S-Impedance - macro model from tomography	Simp_psdmvels.sgy
Lambda*Rho Sections	
Log derived macro model	Lambda_Rho_logvels.sgy
Macro model from seismic NMO velocities	Lambda_Rho_psdmvels.sgy
Sand units predicted by cross-plot – lambda*rho plotted (log velocity model)	Sand_xplot_logvels.sgy
Sand units predicted by cross-plot – lambda*rho plotted (tomography model)	Sand_xplot_psdmvels.sgy
Shale/Pore-pressure Profiles	
Velocity model from tomography + pre-stack inversion	Vel_model.sgy
Predicted shale section with estimated pore pressure (TWT)	Shale_Eaton_pp.sgy
Predicted shale section with estimated pore pressure (Depth)	Shale_Eaton_pp_depth.sgy

"This Project, including data and survey results acquired for the purpose, has been undertaken on behalf of the Porcupine Studies Group (PSG) of the Irish Petroleum Infrastructure Programme Group 3 which was established by the Petroleum Affairs Division of the Department of the Marine and Natural Resources on 15 March 1999 in conjunction with the award of exploration licences under the South Porcupine Licensing Round. The PSG comprises: Agip Ireland BV, Chevron UK Ltd, Elf Petroleum Ireland BV, Enterprise Energy Ireland Ltd, Marathon International Hibernia Ltd, Phillips Petroleum Company United Kingdom Ltd, Statoil Exploration (Ireland) Ltd and the Petroleum Affairs Division of the Department of the Marine and Natural Resources"